

# Quantum efficiency of technical metal photocathodes under laser irradiation of various wavelength

F. Le Pimpec<sup>a,\*</sup>, F. Ardana-Lamas<sup>a,b</sup>, C.P. Hauri<sup>a,b</sup>,  
C. Milne<sup>a,b</sup>

<sup>a</sup>*Paul Scherrer Institute  
5232 Villigen Switzerland*

<sup>b</sup>*Ecole Polytechnique Fédérale de Lausanne  
1015 Lausanne, Switzerland*

---

## Abstract

Quantum efficiency studies for various wavelength and various technical metal surfaces were carried out in a dedicated unbaked vacuum chamber. Copper, magnesium, aluminium and aluminium-lithium photocathodes were irradiated by two different high power, high repetition rate, laser systems. We have observed an emission of electrons for photon energy below the work function of the material. This is explained by multiple photon absorption at the photocathode. We have not observed any degradation of the QE for those materials, but an improvement when irradiating them over a long period of time. This is contrary to observations made in RF photoguns.

*Key words:* Quantum Efficiency, Photocathode, Photoemission, Electron Source,  
*PACS:* 85.60.Ha, 79.60.-i, 29.27.-a

---

## 1 Introduction

In a free electron laser accelerator (FEL) one of the key component is the electron source. The source should provide a sufficient amount of electrons and should have a low emittance to provide the x-ray photons requested by the end users. The electrons can be produced by thermionic emission, photoemission

---

\* Corresponding author

*Email address:* frederic.le.pimpec@psi.ch (F. Le Pimpec).

or by field emission [1,2,3,4]. The successful operation [5,6] of the first x-ray FEL (XFEL) Linac Coherent Light Source (LCLS) using a Cu photocathode has led the Paul Scherrer Institute (PSI) to adapt the LCLS gun design for the future SwissFEL [7,8].

In the meantime, an injector test facility has been commissioned with at its heart a RF photogun using a diamond milled oxygen free electrolytic (OFE)Cu photocathode [9]. The electron production is insured by two different type of lasers, a Nd:YLF (Jaguar<sup>®</sup> by Time-Bandwidth [10]) and a broadband Ti:Sa (Pulsar<sup>®</sup> by Amplitude Technologies[11]) [12]. In order to provide the required electron beam quality (emittance) it is necessary to provide temporally & transversally shaped laser beam. This in turn has an impact on the available laser energy at the cathode. Energy which is needed to produce the amount of charge requested by the machine design [8]. The amount of charges produced by the cathode depends on its quantum efficiency (QE) (number of electron emitted per number of incident photons).

In this technical note, we report on the QE of various metallic photocathodes as a function of the laser wavelength. Cathode ageing is often reported during RF photogun operation [13]. This ageing is characterized by a QE drop, which necessitates to either repair, in-situ, the QE of the cathode or to exchange it [13]. We have then studied the evolution of the QE as a function of the laser irradiation time for several metallic cathodes.

## 2 Experimental setup

The vacuum experimental system is shown in Fig.1. The chamber is sealed using a transparent conflat MgF<sub>2</sub> vacuum window, 90% transmission from 200 nm to 3000 nm. The chamber is pumped through a 50 l/s turbo pump and is not baked. The residual atmosphere is composed of water vapour for more than 95%. The other noticeable peaks are 2 uma, 28 uma and 44 uma. The vacuum is monitored by a compact cold cathode gauge. The pressure during operation is between mid 10<sup>-5</sup> Torr at the start of laser irradiation to mid 10<sup>-7</sup> Torr after a few days of operation. The photocathode insert is placed at the center of the chamber and it is surrounded by a Cu Faraday cup (FC).

The setup can be operated in two ways, shown in Fig.2. Either by biasing the FC and recording the current leaving the insert using a Keithley<sup>®</sup> K6514 Ammeter, or by biasing negatively the insert and recording the current on the FC. A third option would have been to bias negatively the insert and record the current through the K6514; unfortunately the K6514 cannot be used in a floating mode.

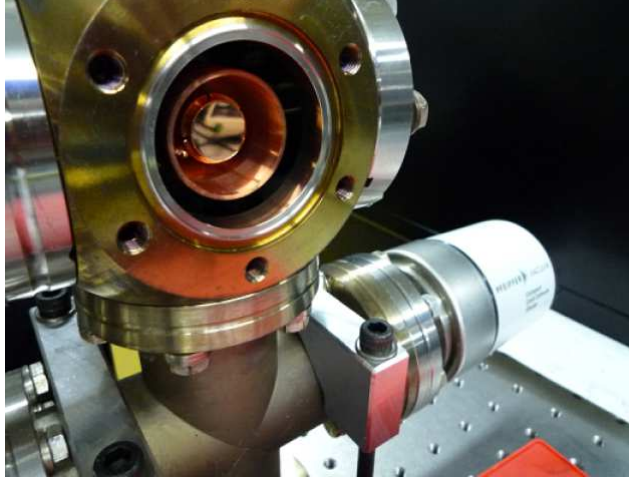


Figure 1. Experimental vacuum chamber with a Cu cathode visible at its center surrounded by a Faraday cup (FC). A cold cathode compact vacuum gauge monitors the total pressure in the chamber. A conflat  $\text{MgF}_2$  vacuum window closes the vacuum chamber.

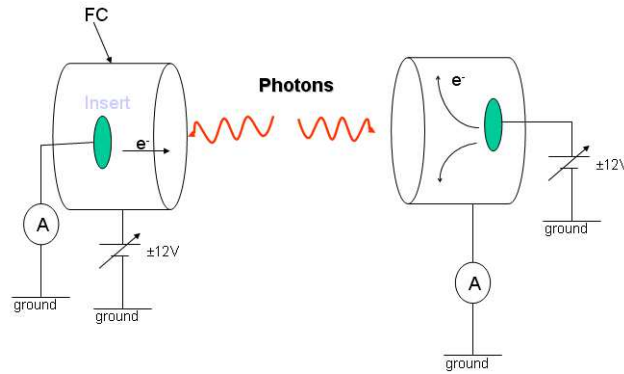


Figure 2. Experimental setup, Electric diagram. The system encompasses an insert (photocathode) a Faraday cup (FC) surrounding it, a  $\pm 12$  V battery powered power supply, and a K6514 Ammeter

We have used two types of lasers. A Ti:Sa working at 800 nm wavelength, 100 fs pulse length with a 1 kHz repetition rate. The 800 nm is sent to a Topas<sup>®</sup> [14] optical parametric amplifier (OPA) system which allows the selection of various wavelength (UV to visible). The fluence used was  $85.6 \mu\text{J}/\text{cm}^2$  with a laser spot diameter between 2 to 3 mm. The laser peak intensity with these parameters was  $0.856 \text{ GW}/\text{cm}^2$ .

The second laser is a Nd:YVO<sub>4</sub>, Duetto<sup>®</sup> from Time-Bandwidth Products [10], working at 355 nm wavelength, with a 10 ps long pulse and a repetition rate set to 200 kHz. The laser average power has been varied from 115 mW to 300 mW depending on the sample. The typical laser spot diameter on target was 8 mm. The laser fluence and peak intensity was, respectively,  $1.2 \mu\text{J}/\text{cm}^2$  ( $0.12 \text{ MW}/\text{cm}^2$ ) and  $3 \mu\text{J}/\text{cm}^2$  ( $0.3 \text{ MW}/\text{cm}^2$ ). Both laser produce linearly

polarized light.

In order to cross-calibrate the K6514 Ammeter, we have measured the current coming from a freshly polished Mg cathode irradiated by the Duetto<sup>®</sup> laser (355 nm; 200 kHz; 140 mW) with a Tektronix-DPO 7254 oscilloscope, using the 1 M $\Omega$  entry impedance. The same cathode, kept under primary vacuum for 3 months, was also illuminated by the Topas<sup>®</sup> laser set to (260 nm, 1 kHz, 5  $\mu$ J), Fig.3.

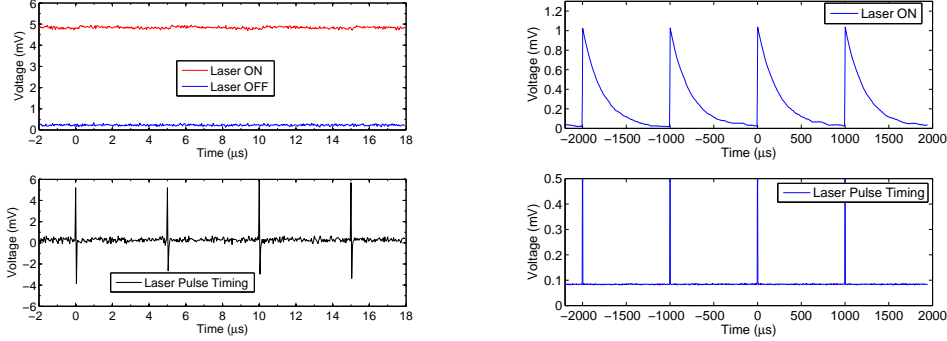


Figure 3. The left figure (top) is the recorded voltage by the oscilloscope when the Mg cathode is illuminated by the Duetto<sup>®</sup> laser (355 nm, 200 kHz, 140 mW,  $\sim 10$  ps), FC = +9 V. A mV corresponding to a nA of photo-emitted current. The right figure (top) is the recorded voltage by the oscilloscope when irradiating the same polished Mg cathode using the Topas<sup>®</sup> laser (260 nm, 1 kHz, 5  $\mu$ J,  $\sim 100$  fs), FC is off. In both figures, the bottom plots are the traces of the recorded laser impulsion.

The comparison shows excellent agreement between the K6514 reading 4.9 nA and the upper trace at 4.9 mV (laser ON) recorded by the oscilloscope, left figure top plot in Fig.3. This 4.9 mV equates to a current of 4.9 nA. The associated QE is  $\sim 0.023$ . The current read by the K6514 is similar, at the % level, when the FC power supply is switched off or when its voltage is set to 0 V via its potentiometer. A zoom in of the laser ON trace will show a small kick every 5  $\mu$ s. This corresponds to the 200 kHz repetition rate pulse of the laser (Fig.3, left figure bottom plot). The oscilloscope cannot resolve the fast current signal produced by the 10 ps long laser pulse, due to the inherent impedance of the whole system. This includes the capacitance of the BNC cable. Consequently, the current displayed by the oscilloscope looks like a DC offset.

In the case of the Topas laser, right plot, the oscilloscope can resolve each pulse. The integrated signal (in nV.s) for one pulse multiplied by the 1 kHz repetition rate is equal, within 5%, to the current recorded by the K6514.

The QE is the number of electrons emitted per irradiating number of photons. The measurement system is not fast enough to resolve the current at every pulse, like commonly achieved in an accelerator. We hence define the QE by

being the number of electrons coming from the average current measured by the K6514 over the number of photons the laser produces in one pulse. A laser delivering 1 mW with 1 kHz repetition rate produces 1  $\mu\text{J}/\text{pulse}$ , and with a 200 kHz repetition rate, 5 nJ/pulse .

### 3 Magnesium and Copper QE vs Wavelength

The intrinsic emittance is the lower limit in beam emittance that one can reach for a given cathode material, surface electric field and laser wavelength. The intrinsic emittance (or thermal emittance) can be expressed as follows, equation 1 [15]:

$$\varepsilon_{\text{thermal}} = \sigma_x \times \sqrt{\frac{h\nu - \Phi_0 + e^{3/2} \cdot \sqrt{\frac{E}{4\pi\epsilon_0}}}{3m_0c^2}} \quad (1)$$

Where the parameters are in SI unit :  $\sigma_x$  the horizontal RMS beam size,  $h\nu$  the energy of the photons (J),  $\Phi_0$  the work function (WF) of a technical metal (J), which differs from an atomically clean surface,  $e$  the elementary charge,  $E$  the applied electric field (V/m),  $m_0$  and  $\epsilon_0$  the rest mass of the electrons and the vacuum permittivity, respectively. In absence of an external electric field, the best emittance is achieved when the photon energy matches the WF of the element, unfortunately when this condition is satisfied the QE drops to zero [15].

From the literature, one can find various WF for different clean metals [16]. The WF of the metals is modified depending on their surface chemistry and crystallographic orientation. Table.1 shows some of the WF for the bare metals we have tested and the associated wavelength ( $\lambda$ ).

#### 3.1 QE vs Wavelength

We have measured the dependency of the QE as a function of wavelength, provided by the Topas<sup>®</sup> OPA, for polished and mirror-like, Cu Fig.4, and Mg Fig.5. According to the theory, we should see a sharp drop of the QE for  $h\nu - \Phi_0 \sim 0$ . During the first experiment the FC was not biased. The pressure during the experiment was in the low to mid  $10^{-6}$  Torr. The QE data are compared to QE measurements obtained in a combined Diode-RF electron gun, labeled (OBLA) and using the RF photogun of the SwissFEL injector, labeled (Injctr).

Table 1

Work function and associated wavelength for some bulk elements [16,17,18,19,20]

Material	Work Function (eV)	Wavelength $\lambda$ (nm)
Mg	3.66	339
Al	4.06 - 4.26	310 - 290
Cu	4.53 - 5.10	274 - 245
MgO	2.8	443
Al <sub>2</sub> O <sub>3</sub>	3.9	318
Cu <sub>2</sub> O	5.2	239
CuO	5.3	234
Laser	4.74 / 4.67 / 3.49 / 2.48	262 / 266 / 355 / 500

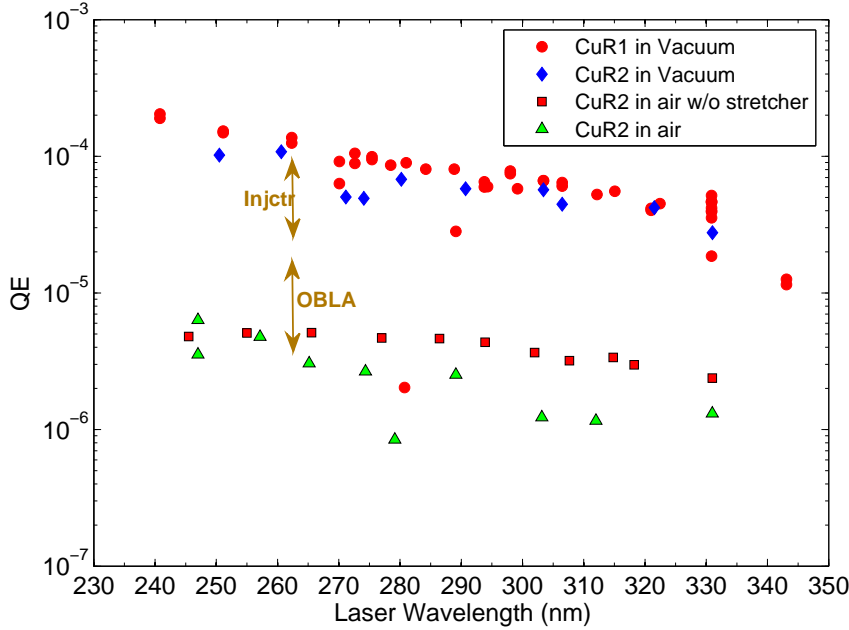


Figure 4. QE vs wavelength of two different polished (mirror-like) Cu samples. The FC is OFF. The QE are compared at a specific wavelength with QE data measured in two different accelerators.

We have redone the experiment on Cu and Mg polished cathodes using two different laser pulse length. The natural pulse length of the Ti:Sapph is  $\sim 100$  fs. Using a glass stretcher the pulse length is elongated to  $\sim 1$  ps. The results for the QE ( $\lambda$ ) presented in Fig.6 have been obtained with the FC set to +8 V. We have insured the collection of all electrons emitted by setting properly the laser energy (in  $\mu\text{J}$ ) at a given wavelength (nm), as shown for example in

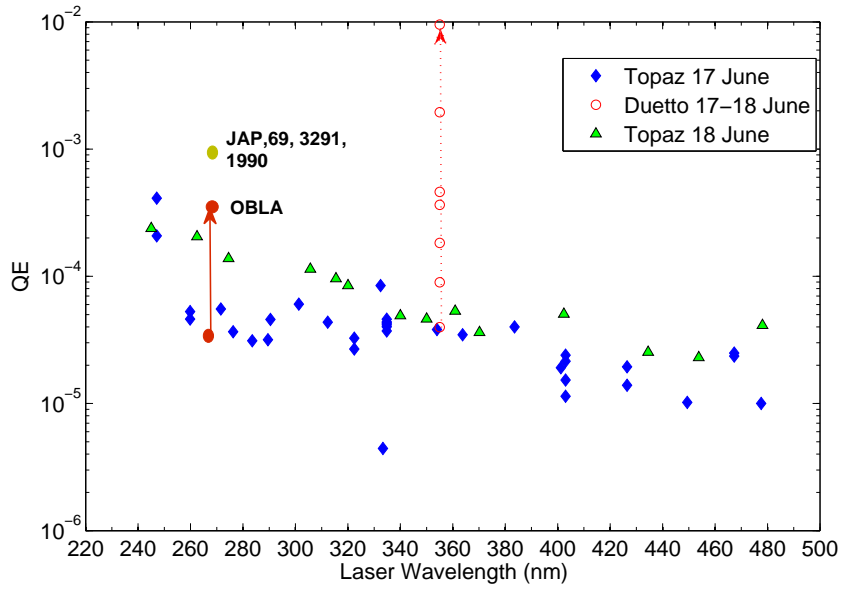


Figure 5. QE vs wavelength of polished (non mirror-like) Mg#2. The FC is OFF.  
Fig.7.

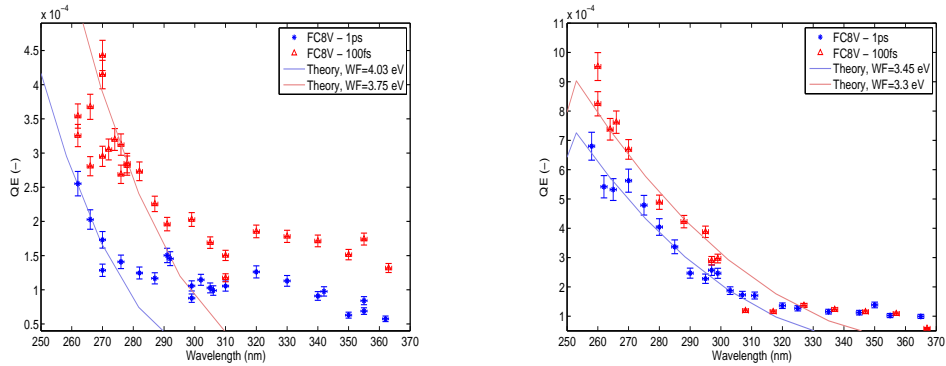


Figure 6. QE vs wavelength of a polished (mirror-like) Cu#R4 sample (left plot) and of a freshly re-polished Mg#2 (right plot), using two laser pulse lengths 1 ps and 100 fs. The straight line are the fittings using equation 2

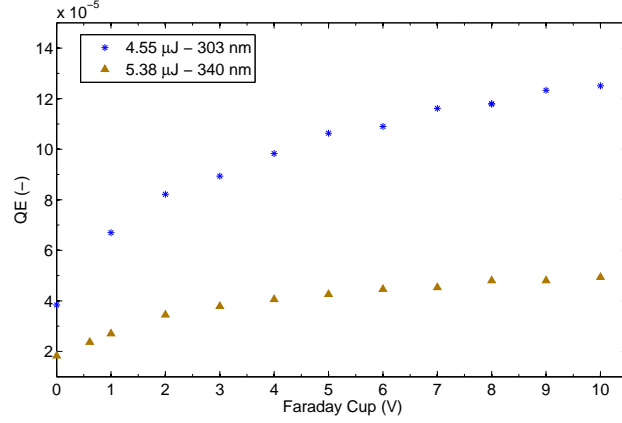


Figure 7. QE of Cu#R4 vs the FC voltage at set wavelength for a set Topas<sup>®</sup> energy in microJ.

### 3.2 Results above the WF

Using the photoemission model described by Spicer [21] and utilizing equation 2 for the  $QE(\lambda)$  [15,22], we have tried to fit the measurements in Fig.6.

$$QE(\omega) = \frac{1 - R(\omega)}{1 + \frac{\lambda_{opt}}{2 \lambda_{e-e}(E_m)} \frac{E_{ph} \sqrt{\Phi_{eff}}}{E_m^{3/2}} (1 + \sqrt{\frac{\Phi_{eff}}{E_{ph}}})} \times \frac{E_F + E_{ph}}{2E_{ph}} \times \left[ 1 - \sqrt{\frac{E_F + \Phi_{eff}}{E_F + E_{ph}}} \right]^2 \quad (2)$$

The validity of equation 2 implies that  $\frac{E_F + \Phi_{eff}}{E_F + E_{ph}} < 1$ , hence a photon energy above  $\Phi_{eff}$ . The equation parameters are as follow. R is the reflectivity,  $E_F$  is the Fermi energy,  $E_{ph} = \hbar\omega$  is the photon energy,  $\lambda_{opt}$  is the laser penetration depth,  $\lambda_{e-e}$  is the electron-electron scattering length and  $E_m$  is the energy above the Fermi level.  $\Phi_{eff}$  is the effective work function, which is the work function  $\Phi_0$  of the bare material minus the barrier reduction due to the external field applied. In our case no strong electric field is present on the cathode, hence  $\Phi_{eff} (eV) \approx \Phi_0$ .

The material reflectivity R, the optical penetration depth  $\lambda_{opt} = \frac{\lambda}{4\pi k}$  are photon energy dependent.  $\lambda_{e-e}$  for Mg has been equaled to  $\lambda_{e-e}$  of Al. In the energy range considered for the escaping electron the mean free path can vary very sharply [23,24].

The parameters used to fit the data for Cu and Mg are summarized in Table.2. For parameters varying in function of the photon energy, a reference is given.

Table 2

Parameters used to fit the QE data for Cu and Mg of Fig.6 [16,22]

Parameters	Cu	Mg
R	[16]	[16]
$E_F$	7 eV	7.08 eV
$\lambda_{opt}$	[16] (nm)	[16] (nm)
$\lambda_{e-e}$	2.2 nm	5 nm
$E_m$	8.6 eV	8.6 eV
$\Phi_0$	3.75 - 4.03 eV	3.3 - 3.45 eV

The fits are rather insensitive to the value of  $\lambda_{opt}$ . According to the above remarks on  $\lambda_{e-e}$ , the fits are sensitive and the work functions  $\Phi_0$  have to be adjusted by 0.1 eV. The reflectivity (R) is a very sensitive parameter. For Mg, there is a gap for R between 3 eV and 5 eV photon energy [16]. The fits shown in Fig.6 (right plot) have been obtained for a constant reflectivity (R=0.72). We have also extrapolated the reflectivity values between 3 and 5 eV. The fits using those value are no more correct. Fitting the data by utilizing equation 2 or the density of states of the material [25] will also show a discrepancy. This is explained as equation 2 is obtained by making use of the free-electron gas model and by approximating the Fermi-Dirac distribution by an Heaviside distribution [15,22].

Finally, The theory seems to fit relatively well the Mg photoemission by assuming a work function which is between the pure Mg metal and its oxide, Fig.6 and Table.1. For Cu, Fig.6 (left plot), one can fit well the data by using WF values below the clean Cu WF (up to 1 eV, Table.1). The meaning of such fit could lead to hypothesize that the Cu surface is contaminated by a chemical elements like an hydride or an alkali. The Mg and Cu samples were installed in the same manner using the same ethanol cleaned tools and gloves. Contamination is unlikely to have occurred.

### 3.3 Results below the WF

We have observed that in all cases, the current recorded did not drop to the noise level of the K6514 when the wavelength of the laser was longer than the wavelength associated with the lowest WF of the clean elements, see Table.1. Sub-ps or ps long laser pulse seems to affect the surface so that photoemission is possible for wavelength longer than the photoemission wavelength threshold. When comparing the QE, for Mg or Cu, at pulse length of 100 fs and 1000 fs, The QE differs only a little, Fig.6. Nevertheless it seems interesting to look at

different mechanism which could explain the electron emission at wavelength above the material WF. Do we have :

- \* Thermal effects ?
- \* Plasmonic effects ?
- \* Multi-photon absorption ?
- \* Mechanical effect (stress, strain) ?
- \* Chemistry (oxide effect) ?

### 3.3.1 Thermal effects

The increase of temperature due to the laser irradiating the inserts can be calculated using equation 3:

$$Q = m \times C_s \times \Delta T \quad (3)$$

where  $Q$  is the heat energy (J),  $C_s$  is the specific heat (J/(kg.K)) and  $m$  the mass of the material (kg). We use at most  $10\mu\text{J}$  of laser energy in the UV spectrum per pulse. We assume that all the laser energy is converted into heat. We have also considered, in Table.3, that the UV light ( $\sim 5 \cdot 10^{15}$  Hz) heats only a very thin layer of the insert (skin depth)  $\sim 1$  nm thick, over the whole sample surface. If one assumes that only the skin depth under the irradiated area of the laser is heated then the temperature increase will exceed 900 K, which is enough to melt Mg and Al. We have not observed any damages on polished mirror-like samples. However, we have observed a dark spot under an optical microscope for the Mg, Fig.8. This black spot can also be observed on Mg cathodes which have undergone laser cleaning in the combined Diode-RF electron gun (OBLA) [26], Fig.9. In the OBLA experiment, we have rastered the laser beam on the Mg surface. The laser fluence could be up to  $40 \text{ mJ/cm}^2$  at 266 nm, using a 10 ps long laser pulse with a repetition rate of 10 Hz. The diamond area cleaned, Fig.9, was obtained using  $12 \text{ mJ/cm}^2$  of laser fluence. In the small chamber experiment, the fluence of the Topas<sup>®</sup> and Duetto<sup>®</sup> on Mg#2 were respectively less than  $85 \mu\text{J/cm}^2$  (2-3 mm laser spot size) and  $1.2 \mu\text{J/cm}^2$  (8 mm laser spot size).

From the consideration above, we think that thermal effects cannot account for the emission of light for laser energy below the work function.

### 3.3.2 Plasmon assisted photoemission

Surface plasmon can enhance the photoemission of surfaces [27,28,29,30]. The photoemission enhancement occurs for some angle of incidence and is also

Table 3

Temperature increase of different metals when submitted to  $10 \mu\text{J}/\text{pulse}$  laser irradiation.

Metals	Mass (kg)	Specific Heat (J/(kg.K))	$\Delta T$ (K)	$\Delta T$ ( $\sim 1 \text{ nm}$ ) (K)
Cu	0.0028	387	$9.2 \cdot 10^{-6}$	19
Mg	0.0021	1050	$4.5 \cdot 10^{-6}$	23
Al	0.0014	900	$7.9 \cdot 10^{-6}$	42

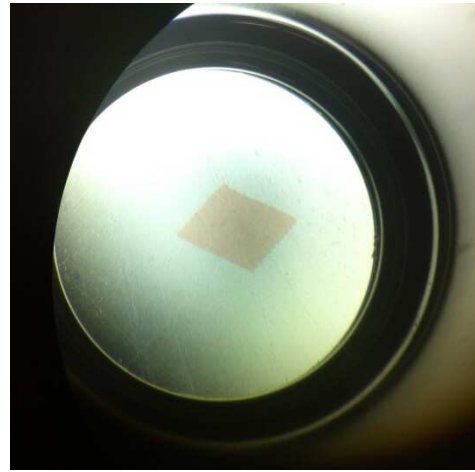
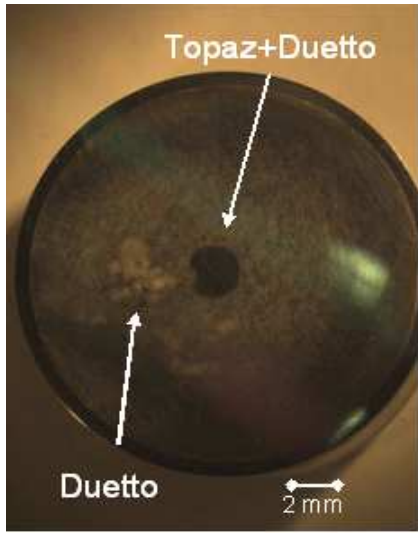


Figure 8. Damages caused by laser expo- Figure 9. Damages caused by laser clean-  
 sion on polished but rough Mg# 2 ing on polished Mg in the combined  
 Diode-RF gun (OBLA)

polarization dependent. We operate at normal incidence, and both lasers are linearly polarized in the plane of the photocathode. At normal incidence the probability of plasmon excitation is usually quasi null [28]. However, it seems that when the roughness of the surface is on the order of a few 10's of nanometers, surface plasmon could be excited hence enhancing photoemission [31].

### 3.3.3 Mechanical effect (stress, strain)

All of our inserts are mechanically polished. This induces stresses in the metal and on its surfaces. After polishing, the inserts are not baked, hence not stress relieved. Mechanical stress has been shown to modify the WF of metals [32]. However, the modification seems not to be sufficient to account for the photoemission at photon energy below 4.1 eV.

### 3.3.4 Chemistry on the surface

The presence of oxygen on the surface can significantly modify the the WF of a bare metal, either by lowering it or by increasing it [17,33,34]. Although contaminant layers produced by air exposure are usually detrimental to the QE [13,35], applying a thin film of MgO over silver can not only lower the Ag work function but may also be beneficial for the electron beam emittance in an accelerator [36].

We believe that some part of the photoemission curve for Mg, Fig.5, can be explained by the presence of the oxide. On the contrary natural copper oxide seems to have a work function above 5 eV [18], hence a detrimental oxygen chemistry compared to Mg.

### 3.3.5 Multiphoton absorption

Multi-photon absorption, mainly two-photon absorption, is possible if the density of photons impinging the surface is high enough. Both laser Topas<sup>®</sup> and Duetto<sup>®</sup> can deliver such intensities. Fig.10 shows the intensity of current extracted from Cu at 253 nm and at 331 nm for Topas<sup>®</sup> pulses of 100 fs and 1 ps.

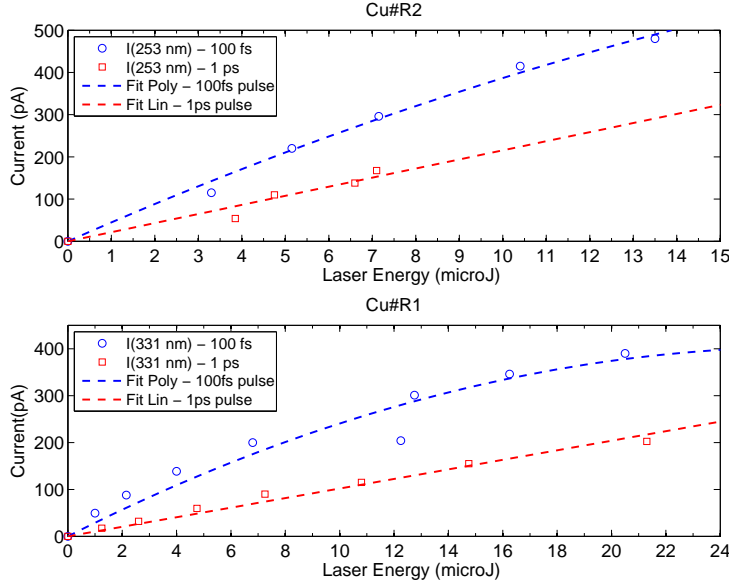


Figure 10. Electron Current extracted versus the Topas<sup>®</sup> laser energy at 253 nm for CuR2 and at 331 nm for CuR1. In both cases the FC is OFF.

For photon energy above the WF, like for  $\lambda=253$  nm, one should expect to see a linear dependence of the current vs the laser energy. For photon energy below the WF, for  $\lambda=331$  nm, one should see a quadratic dependence of the

current vs the laser energy. For Cu, for both wavelength, we have a linear dependency of the current emission versus the laser energy for laser pulse length of 1 ps. For laser pulse length of 100 fs, the dependency seems quadratic. However, the quadratic dependence should have a positive bending and not a negative one as shown. This quadratic negative bending dependence is often seen in RF photogun when the bunch space charge hampers the emission of electrons [13]. A linear fit through zero can also be satisfactorily applied for Cu#R2 irradiated at 253 nm with a 100 fs laser pulse length. This fit implies an electron emission by a one-photon photoelectric effect which is non space charge limited.

For Mg#2, we have measured the current emission vs the laser energy. For  $\lambda=247$  nm the dependance is linear. For the following wavelength  $\lambda$  (403 nm, 520 nm) the dependance is quadratic with a positive curve, hence implying a photoelectric effect driven by a double-photon absorption.

### 3.4 Comparison with other data

We have compared the data obtained in this chamber with data obtained inside an RF photogun. For Cu it is usual to find values for the QE in the  $10^{-5}$  range. We measured similar values in our combined Diode-RF gun, labeled OBLA in Fig.4, and in our RF photoinjector, labeled Injctr in Fig.4. At 250 nm, QE value of  $1.4 \cdot 10^{-4}$  is also reported. This is consistent with our measurements [13,37,38].

We have also reported some of the QE data obtained on bulk or thin film Mg obtained in our combined Diode-RF gun, labeled OBLA. The results obtained are compatible with literature data [13,31,35,39].

## 4 Duetto laser cleaning

### 4.1 Cu and Mg

At 355 nm we have measured the QE of Mg#2 using the Duetto<sup>®</sup> laser, Fig.5 (circles). The chamber was partially vented to 0.1 mbar of air atmosphere during the transfer of the chamber from one location to another. The initial QE is similar to the QE measured with the Topas<sup>®</sup> laser. The QE increases with the irradiation time. The laser spot size was chosen to be 8 mm in diameter on the cathode with a fluence of usually  $1.2 \mu\text{J}/\text{cm}^2$ . The fluence per pulse is  $\sim 80$  times lower that when using the Topas<sup>®</sup>. Fig.11 (left) shows the cur-

rent extracted from two polished Cu cathodes, which were HCl cleaned to remove the oxide layer and then rinsed with alcohol before mounting. Fig.11 also shows the current extracted from a polished and mirror-like Mg photocathode (Mg#7) for comparison. The laser peak intensity, associated to the laser energy, varies from 0 to  $0.45 \text{ MW.cm}^{-2}$ . The QE in function of the laser energy is shown on the right plot of Fig.11. For the Cu cathodes, the data plotted were measured while the FC was set to +4 V and 0 V for Mg#7 cathode. Fig.12 and Fig.13 show the effect on the current/QE measured when applying a small positive voltage on the FC.

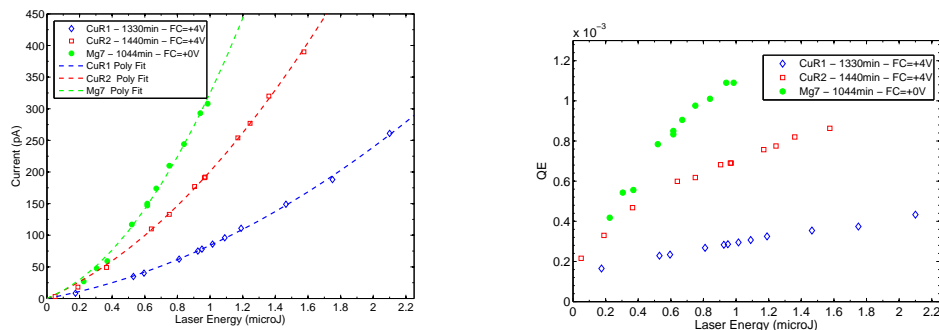


Figure 11. Current (left) and QE (right) measured as a function of the Duetto<sup>®</sup> laser energy for two Cu samples and one Mg insert. Double-Photon absorption emission is responsible for electron emission For Cu the FC is on at +4 V and is off for the Mg insert.

The electron current measured while irradiating at 355 nm wavelength, 10 ps pulse length, is due (for Cu and Mg) to the double-photon absorption, square fitting of the current vs the laser energy in Fig.11. We have seen no black marking like in Fig.8, on either Cu or Mg samples. The samples stayed pristine after a few days of irradiation. The conditioning in time of Cu was carried out with the Duetto<sup>®</sup> laser delivering 200 mW of power, while being 130 mW for Mg#7.

As already mentioned, Fig.12 and Fig.13 show the effect on the current/QE measured when applying a small positive voltage on the FC. The increase of current extracted is usually above a factor 10 when applying a few Volts on the FC.

The total vacuum pressure of the unbaked vacuum system during the laser exposure (2300 min) dropped from  $5.10^{-5}$  Torr to  $5.10^{-6}$  Torr. The evolution of the QE for Cu, goes from the mid  $10^{-6}$  range to the mid  $10^{-5}$  range when the FC power supply is turned off, data not shown. The QE, FC ON, for Cu is  $\sim 0.1\%$  (Fig.12) and  $\sim 4.5\%$  for Mg (Fig.13). Those QE are much higher than the QE measured for photocathodes installed in an RF photogun. This is explained by the fact that in an accelerator the charge per bunch, hence per laser pulse, is accurately measured, while here we measure the average

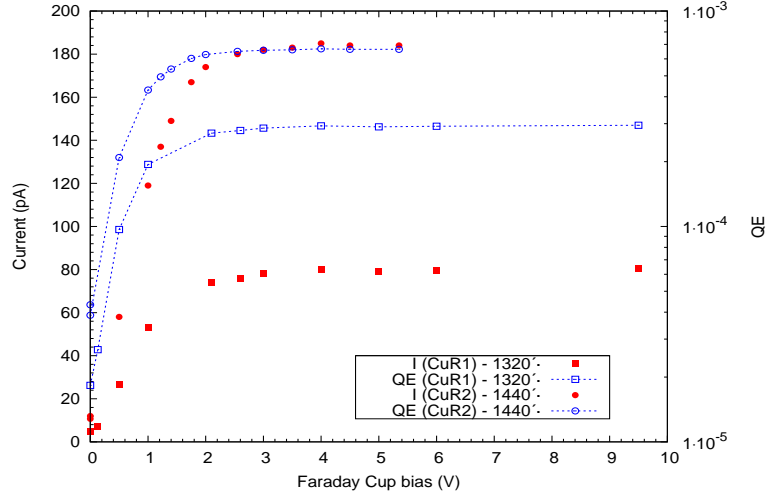


Figure 12. QE and Current versus the FC bias of two polished mirror-like Cu samples

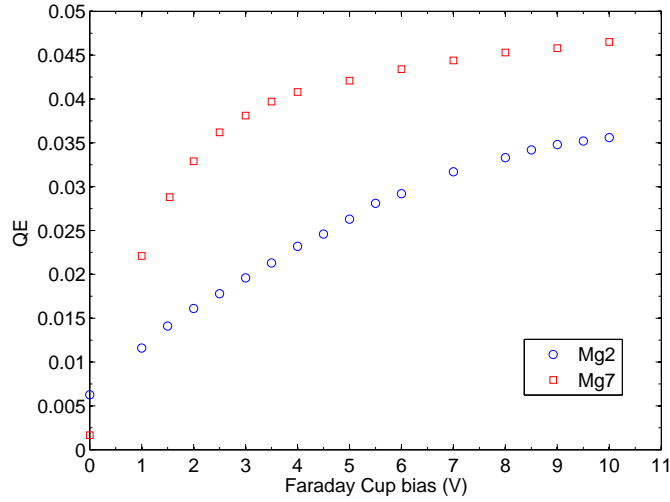


Figure 13. QE versus the FC bias of two polished Mg sample Mg# 2 (rough) and Mg # 7 (mirror-like)

current.

The volume of interaction between the residual gas and the laser beam is of a few  $\text{cm}^3$ . The number of molecules at  $10^{-6}$  Torr and in a  $\text{cm}^3$  is in the order of  $3 \cdot 10^{10}$  and the number of photons in the beam is  $\sim 3 \cdot 10^{12}$ . The usual cross section of interaction is  $10^{-16} \text{ cm}^2$ . This would amount to a pA of current, if all ions were falling on the photocathode. The main effect of the FC bias is the suppression of the space charge present at the cathode surface hampering the emission of electrons. This space charge is weak enough that only a few Volts are sufficient to counterbalance it, as shown by the current plateau for bias above +4 V, Fig.12.

We have also monitored the evolution in time of the QE for Mg cathodes

when irradiated by the Duetto<sup>®</sup> at 355 nm, Fig.14. The laser size on cathode was 8 mm and the repetition rate 200 kHz for all the data plotted. The full diamond plot labelled "Mg2 Jun2010" is the same data plotted in Fig.5 (open circles). The laser cathode cleaning with low energy per pulse increases the QE by a few order of magnitude after less than 10 hours of exposure. The laser was blocked for one hour and the system kept in vacuum. Upon restart the QE barely dropped. The same cathode was reused 6 months later. The cathode was left in the vacuum chamber, which was air-vented and the vacuum valve was closed. After pump down, the laser was shined on the cathode with the same parameters as used previously, including an average power of  $\sim 130$  mW; open square data labelled "Mg2 Jan2011". The QE almost reached the same value as before in the same amount of time. The laser was blocked over night, with the vacuum pressure improving during the night. Again the drop in QE was minimal upon resuming irradiation. Damages, on the polished but non-mirror like sample, from the irradiation by both lasers have been shown in the left photo of Fig.8.

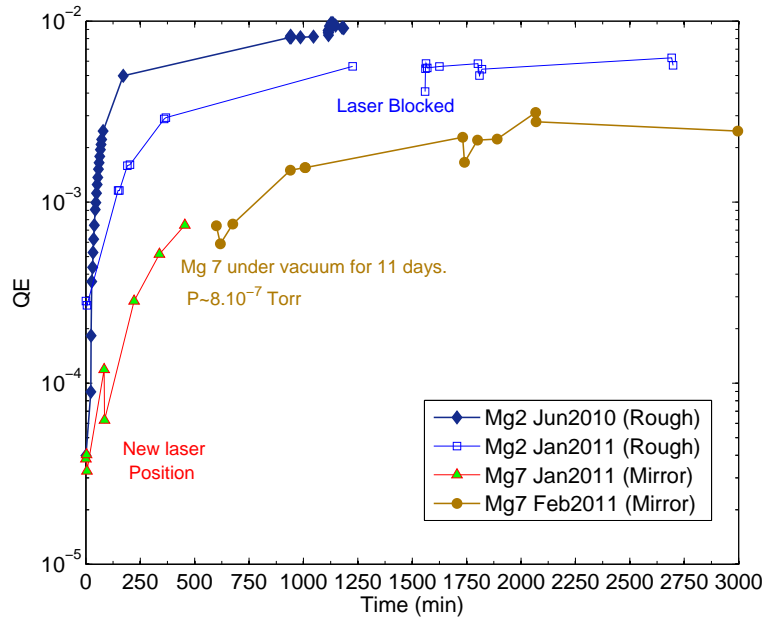


Figure 14. QE evolution under Duetto irradiation for two polished Mg sample Mg#2 (rough) and Mg#7 (mirror-like). FC is off in all cases.

A freshly polished Mg (Mg#7) insert was installed in the vacuum chamber, and exposure started when the surrounding pressure was  $\sim 5 \cdot 10^{-5}$  Torr. The parameters used for the irradiation were similar to the one used for sample Mg#2. The first QE value recorded was lower than for a rougher surface. This is not surprising as rougher surfaces will trap more photons, hence increasing the production of electrons compared to a flatter surface. The QE of the mirror-like surface stays systematically lower than for a rougher surface.

After a couple of hours of irradiation on Mg#7, Fig.14 (full triangle), the laser spot was moved to another location on the cathode. The sample size was 14 mm and the spot size was 8 mm. It is possible that some overlapping of the already conditioned area occurred. This would explain why the QE reduction seen does not fall at the starting value. After a few more hours of laser exposure, the laser was taken away and the system kept in a dynamic vacuum for 11 days. After re-start of the illumination (full circle), the QE value of Mg#7 is similar to the end-of-illumination QE value (full triangle), Fig.14 .

It seems to be commonly acknowledged that long exposure to the vacuum residual gas is detrimental to the QE [35]. This result on Mg and some more on Cu (Fig.20) and AlLi (Fig.15) are in flagrant contradiction.

Using a high repetition rate, short pulse laser, with a wavelength longer than the associated wavelength of the WF, at a low fluence (less than a microJ of energy per pulse over a "broad" area), in an unbaked vacuum atmosphere has proven efficient in increasing the QE of both Cu and Mg cathodes. In both cases multi-photon absorption is responsible for electron emission. In the case of Mg, Mg oxide can have a lower work function than pure Mg and the emission at 355 nm can be normal photoemission instead of double-photon absorption. After a few hours of laser exposure, we have not seen any linear dependence of the current extracted versus the laser energy.

#### *4.2 Aluminium and Aluminium Lithium alloy*

Similarly to what was done on copper and magnesium, we have irradiated an aluminium (Al) sample and an Aluminium Lithium (AlLi) alloy insert.

Al and AlLi photocathode could be alternatives to Mg as a photocathode. In the Diode-RF electron gun (OBLA) we have measured the emittance and the QE of various metals [13,26,40]. Respective to the QE, Aluminium has been found better than Copper and not as good as Magnesium. The emittance was higher than for Cu. According to literature Mg also produces lower emittance than Cu [31]. What could make Al still attractive, is its higher vapour pressure upon baking compared to Mg. Most photo-RF guns are baked before RF processing is started, although the temperature might be less than 150 C for a long period of time.

As an alternative to pure Al is AlLi alloy [41]. Lithium and Magnesium are in the first and second group of the periodic table. They are both strongly reactive to oxygen. Both elements might migrate on top of the surface of Al over time [42] which might be the reason for the enhanced production of electrons compare to the bare Al.

$\text{Al}_{95}\text{Li}_{2.5}\text{Cu}_{1.5}\text{Mg}_1$  alloy was bought from Goodfellow<sup>®</sup> in tube form. The tube was smashed into a circular insert then polished (mirror surface like) and kept in air for 3 months before installation.

The irradiation with the Duetto<sup>®</sup> laser produced only a few pA of currents, independently of the FC voltage) even when using 380 mW of laser power, fluence  $3.8\mu\text{J}/\text{cm}^2$ . The current extracted did decrease from 3 pA to 1 pA in 20 min. The sample was sent to polishing and re-installed. The results of the current and QE obtained at different times of exposure versus the FC voltage are shown in Fig.15.

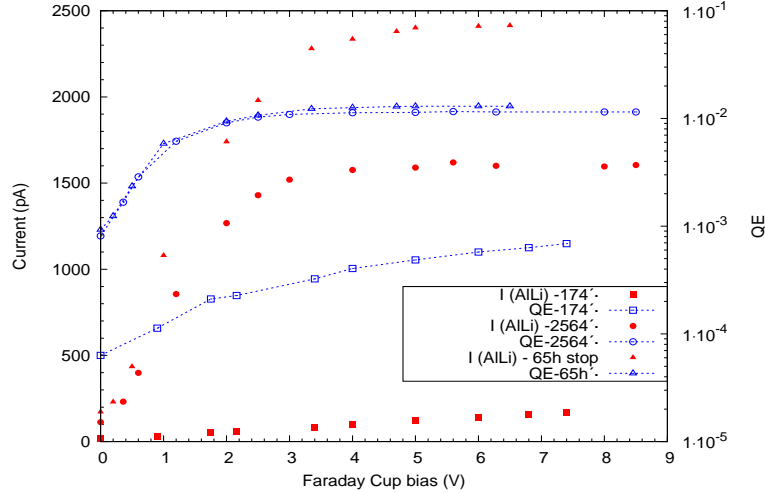


Figure 15. QE and Current evolution of AlLi alloy during Duetto<sup>®</sup> exposition, in function of the FC bias voltage.

The production of electrons is done through the double-photon absorption process as seen by the square dependency fit in Fig.16. The data labelled "65h stop" on both figures, Fig.15 and Fig.16, have been obtained at re-start of irradiation after 65 hours of laser downtime. During that time the chamber stayed actively evacuated by the vacuum pump system. As for Cu or Mg, the QE of the AlLi did not decrease while the sample stayed in an unbaked vacuum ( $P \sim 2.6 \cdot 10^{-6}$  Torr) for a few days.

For extracted current above 1500 pA, during the QE vs FC voltage scan, and after every step up of the FC voltage the current reads high and can drop by 100 pA in 30 s. For extracted current below 1500 pA, the current drops by a few pA. After this initial drop in extracted current, the charge extracted increases again slowly under the Duetto<sup>®</sup> irradiation. This behaviour, initial extracted current drop after an increase of laser power, was not observed on either Cu or Mg.

Finally we tested a freshly polished Al sample. The QE and current extracted versus the FC bias is shown in Fig.17, at different times of laser exposure. A previous attempt of measuring the QE vs wavelength on an Al sample kept in

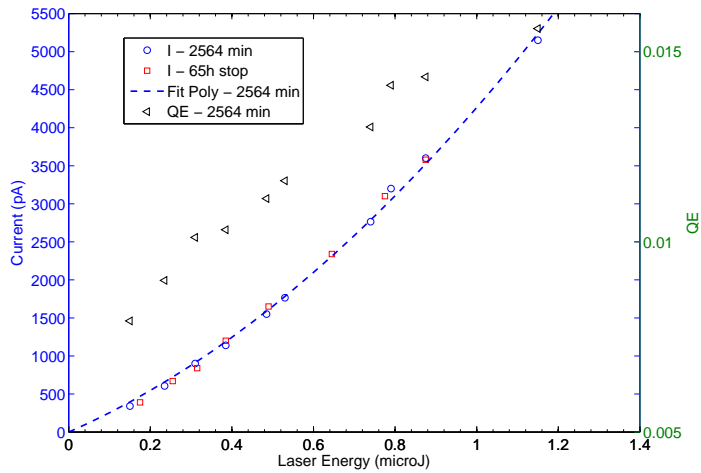


Figure 16. AlLi current extracted in function of the Duetto<sup>®</sup> laser energy. FC is set at +4V.

air for a long time did not give consistent results as were obtained for Cu or Mg, Fig.4 and Fig.5.

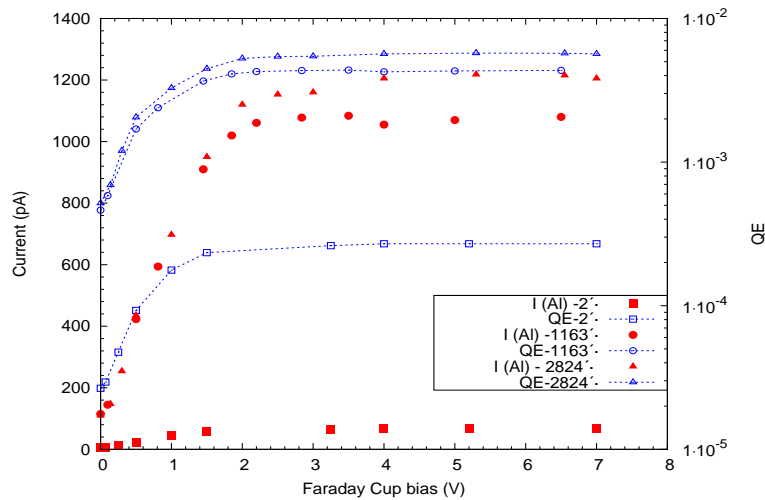


Figure 17. QE and Current evolution of Al during Duetto<sup>®</sup> exposition, in function of the FC bias voltage.

Al and AlLi alloy reacted similarly in terms of QE. The initial QE, FC OFF, is in the  $10^{-5}$  range and increases by a decade at the end of the laser exposure. When turning on the FC, the end value for the QE (for AL and AlLi) is close to a percent. In both cases the photoemission is double-photon absorption. It seems that for Aluminium-based photocathode, a freshly prepared cathode behaves better than a cathode well prepared and then kept in air for a few months. This was not seen for Mg or Cu. No damage was seen on either Al or AlLi sample after removal from the chamber.

## 5 Ageing of Cu

LCLS has shown that a high current, XFEL operation compatible emittance, can be obtained from a well-prepared Cu photocathode. A long lifetime between cathode exchange is also beneficiary for user operation. However, as the cathode ages the QE drops and in-situ techniques, like laser cleaning, can be applied to regenerate the QE. On the right photograph of Fig.8, we have seen how an aggressive laser cleaning can modify the surface. Laser induced surface alteration was also seen on the Cu cathode of LCLS or in the SPARC experiment [13].

The ageing of the cathode is characterized by the formation of a QE hole, or a charge hole, as shown in Fig.18. Fig.19 shows the QE evolution in time of one Cu cathode (Cu\_3) and is compared to the QE of another Cu photocathode (Cu\_1) after a year of operation.

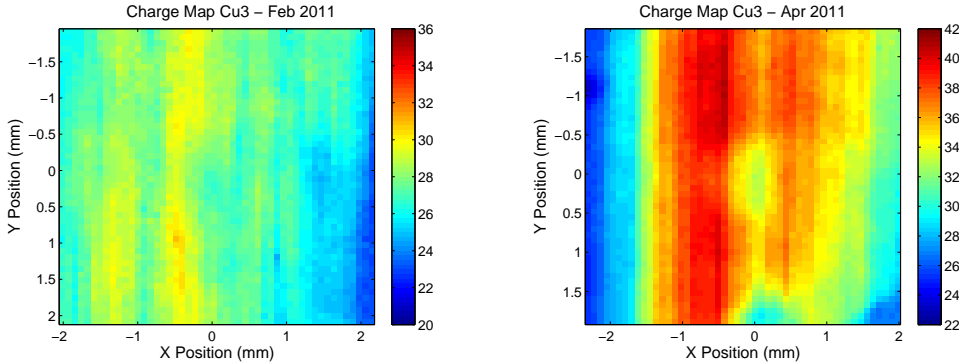


Figure 18. Charge map (pC) evolution of the Cu photocathode (Left plot: initial charge map) after three months of Injector operation (right plot).

We were able to illuminate some Cu cathodes using a high repetition rate UV laser producing a low fluence on the surface. What we observed was an increase of QE with time.

At the PSI injector, the UV lasers work at a low repetition rate (10 Hz); and this until the end of the commissioning period. The two lasers used at the injector Jaguar<sup>®</sup> or Pulsar<sup>®</sup> are set to operate with a 10 ps long pulse, at wavelength of  $\lambda=262$  nm or 270 nm. The laser spot size is 1 mm on target. We typically use 10-20  $\mu\text{J}$  per pulse, hence a Fluence of 1.27 to 2.55  $\text{mJ}/\text{cm}^2$  and a power density of 127 to 255  $\text{MW}/\text{cm}^2$ .

In order to reproduce the QE hole in the small system chamber, we have used the Topas<sup>®</sup> laser with the following settings : 1000 Hz repetition rate, 1 ps long pulse,  $\lambda=261$  nm, a laser spot size between 1 to 1.2 mm on target. The energy per pulse was 9  $\mu\text{J}$  so a Fluence between 0.8 to 1.15  $\text{mJ}/\text{cm}^2$  and a power density between 800 to 1150  $\text{MW}/\text{cm}^2$ . The QE and current measured during the laser exposure of a Cu insert are shown in Fig.20. The already

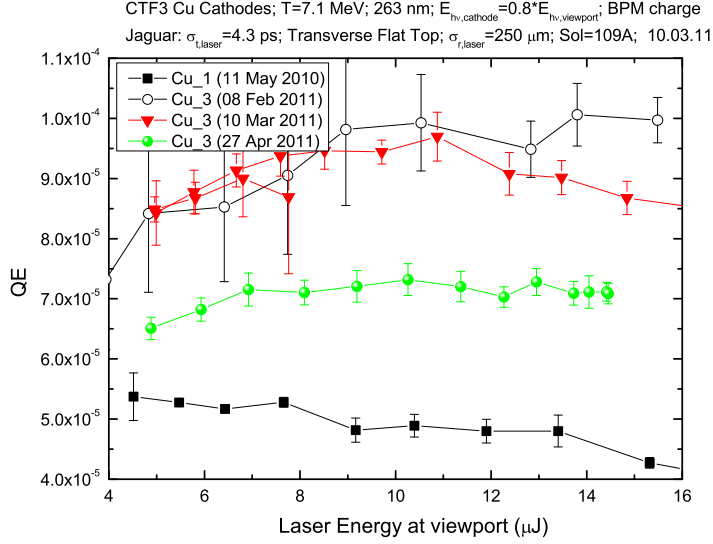


Figure 19. New Cu photocathode (Cu<sub>3</sub>) QE evolution after three months of Injector operation. Comparison with the QE of the first cathode installed Cu<sub>1</sub> [43].

used Cu sample (CuR2) was installed after an ethanol wipe. The sample was exposed to the Duetto<sup>®</sup> laser 90 days before this experiment, and was stored in air during that time. Any exposure to air cancels any effects from a laser conditioning/cleaning.

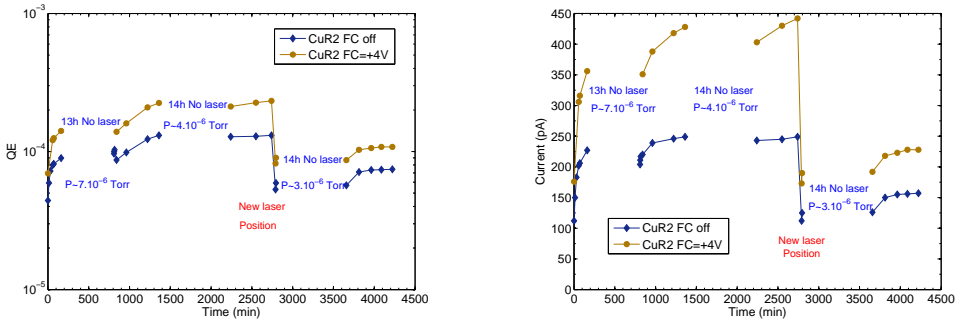


Figure 20. QE (left) and Current (right) measured from a Cu cathode (CuR2) using the Topas<sup>®</sup> laser with a 1 kHz repetition rate and with  $\lambda=261$  nm

The Topas<sup>®</sup> was not available during nights, hence the gaps in the conditioning curve in Fig.20. The injector operation is also usually stopped during nights. The overall time of the laser on target is  $\sim 20$  hours. The fluence in the small chamber is, in the worse case, 70% of the injector gun fluence. This amount for an equal time of 58 days of injector operation. By that time, we should have seen a degradation of the QE, and not an improvement as seen on the left plot of Fig.20.

We then moved the laser spot to another location on the cathode and have further reduced the laser spot size to 0.7 mm. The initial QE,  $t=2790$  min, is

similar to the first starting point at  $t=0$  min. The QE did increase but then seemed to level off after a few hours of operation. The laser energy was constant to  $10 \mu\text{J} \pm 1.5 \mu\text{J}$ . The sample CuR2 showed no surface damage upon removal from the chamber.

We changed the sample by another Cu insert, which was also previously used and stored in air. We irradiated this sample using the Duetto<sup>®</sup> laser with its wavelength set to 266 nm, with 200 kHz repetition rate. The spot size was set to 0.4 mm in diameter, and the fluence used decrease from initially  $255 \mu\text{J}/\text{cm}^2$  to  $65 \mu\text{J}/\text{cm}^2$ . At high fluence the sample produced up to 7 nA of current with the FC set at +4 V and a couple of nA with an off voltage on the FC. We probed a different location on the insert with a lower laser fluence. The laser beam size was sufficiently small to avoid any overlap on a previously irradiated area. Again, we have seen no sign of QE degradation but on the contrary a QE increase, even after 3 continuous days of irradiation at 200 kHz (266 nm).

We can only hypothesize about the reasons why we could not degrade the QE. Our RF photogun is baked to 120 C during almost a week. Hence a different vacuum spectrum than an unbaked vacuum system. In the baked case the vacuum spectrum is dominated by the hydrogen peak (2 uma) and not by water. The cathode in the electron gun is submitted to a high power (20 MW) and high gradient (100 MV/m) of RF field alternating at 3 Ghz. This RF field produces dark current and ions. Both can strike back the cathode and degrade the QE. However, Fig.19 (right plot) still shows a mostly homogeneous QE over the whole cathode.

The vacuum environment of our system is at first dominated by water (>95%). It is then possible that the intense laser light cracks the water molecules, producing very reactive radicals. These radicals would continuously restore the QE, as does an Ozone cleaning [13]. The pressure is usually in the  $10^{-6}$  Torr range. At this pressure a monolayer is formed every second. Laser heat can also activate surface molecule diffusion, and maybe the re-arrangement at this pressure of the oxide layer is beneficial, although the mechanisms are unclear. However, one should note that the vacuum spectrum of an unbaked system can be similar, qualitatively, to a baked system; if one allows the vacuum chamber to be pumped long enough.

## 6 Conclusion

It seems a good idea to measure the work function of a technical metal using an infrared laser coupled with an optical parametric amplifier. However, as we have seen in Fig.4 the QE (or extracted electron current) decreases but do not drop sharply for wavelength longer than the work function. This would be

what one would expect after experimenting with a powerful UV lamp coupled to a monochromator. Double-photon absorption leading to photoemission was put in evidence for a UV laser with a long emission pulse (10 ps) on Al, AlLi, Cu, and Mg; ( $\lambda_{Laser} > \lambda_{WF}$ ). We were not able to determine the cause of the photoemission when using ps or shorter laser pulse length.

We have observed that a UV (266 nm and 355 nm) high repetition rate laser (1 kHz or 200 kHz) shined on various metallic surfaces located in an unbaked UHV vacuum environment is beneficial to the QE, as it increases it. These results are in agreement with the results obtained using aggressive laser cleaning procedure applied on photocathodes for RF photoguns. We observe, contrary to laser cleaning techniques, that the mirror-like polished surfaces stay pristine after our extensive but not aggressive laser exposure.

We were not able to reproduce the QE hole which is commonly seen on RF photoguns' photocathodes after many hours of operation, in spite of the use of laser parameters similar to parameters used for electron production at the PSI photogun. We attribute this fact to probably the most important parameter, the absence of the RF field. Secondly to the difference of vacuum composition between a baked RF photogun, which mainly contains hydrogen, and our unbaked system which predominantly contains water. We hypothesize that the water molecules are cracked by the laser beam on the photocathode and that the radicals produced enhance the QE instead of being detrimental to it.

## 7 Acknowledgments

S. Ivkovic for polishing the numerous test samples, sometimes on short notice. The SLS vacuum group and pulse magnet group for lending some equipments and providing knowhow. The FEMTO group for allowing us to use their lasers during the SLS shutdown. M. Divall for valuable discussion and F. Celli for proofreading this text.

## References

- [1] R. Ganter, R.J. Bakker, C. Gough, F. Le Pimpec, M. Paraliiev, M. Pedrozzi, L. Rivkin, A.Wrulich. Nanosecond field emitted and photo-field emitted current pulses from ZrC tips. *Nuclear Instruments and Methods in Physics Research A*, 565:423–429, 2006.
- [2] K. Togawa, T. Shintake, T. Inagaki, K. Onoe and T. Tanaka. CeB<sub>6</sub> electron gun for low-emittance injector. *Phys. Rev. Special Topics - Accelerators and Beams*, 10 (020703), 2007.

- [3] Y. Ding et al. Measurements and Simulations of Ultralow Emittance and Ultrashort Electron Beams in the Linac Coherent Light Source. *Phys. Rev. Lett.*, 102:254801, 2009.
- [4] F. Loehl et al. High Current and High Brightness Electron Sources. In *IPAC2010, Kyoto, Japan*, 2010.
- [5] P. Emma et al. "First lasing and operation of an Ångstrom-wavelength free-electron laser. *Nature Photonics*, 4:641, 2010.
- [6] G. Doumy et al. Nonlinear Atomic Response to Intense Ultrashort X Rays. *Phys. Rev. Lett.*, 106:083002, 2011.
- [7] B.D. Patterson et al. Coherent science at the SwissFEL x-ray laser. *New Journal of Physics*, 12-035012, 2010.
- [8] R. Ganter, editor. *SwissFEL Conceptual Design Report*. PSI-10-04. 2012.
- [9] T. Schietinger et al. First Commissioning Experience at the SwissFEL Injector Test Facility. In *LINAC10, Tsukuba, Japan*, 2010.
- [10] Time-Bandwidth products. <http://www.tbwp.com/>.
- [11] Amplitude Technologies. <http://www.amplitude-technologies.com/>.
- [12] C. Vicario, R. Ganter, F. Le Pimpec, C.P. Hauri, S. Hunziker, C. Ruchert, T. Schietinger and A. Trisorio. Photocathode Drive Laser for SwissFEL. In *FEL10, Malmö, Sweden*, 2010.
- [13] Workshop on Photocathodes for RF Guns, 2011. <http://photocathodes2011.eurofel.eu/>.
- [14] Light Conversion. <http://www.lightcon.com/>.
- [15] D.H. Dowell and J.F. Schmerge. Quantum efficiency and thermal emittance of metal photocathodes. *Phys. Rev. ST : Accel & Beams*, 12:074201, 2009.
- [16] W.M. Mickey Haynes, editor. *Handbook of Chemistry and Physics*. 92<sup>nd</sup> edition. CRC PRESS, 2012.
- [17] R.A. Chapman. Thermionic Work Function of Thin-Oxide-Coated Aluminum Electrodes in Vacuum and in Cesium Vapor. *Journal of Applied Physics*, 35(10), 1964.
- [18] J.A. Assimos and D. Trivich. The Photoelectric Threshold, Work Function, and Surface Barrier Potential of Single-Crystal Cuprous Oxide. *Phys. Stat. Sol.*, (a) 26:477, 1974.
- [19] F.P. Koffyberg and F.A. Benko. A photoelectrochemical determination of the position of the conduction and valence band edges of p-type CuO. *Journal of Applied Physics*, 53(2):1173, 1982.
- [20] B. Brennan, S. McDonnell and G. Hughes. Photoemission studies of the interface formation of ultrathin MgO dielectric layers on the oxidised Si(111) surface. *Journal of Physics :Conf. Series*, 100:042047, 2008.

- [21] W.F. Krolikowski and W.E. Spicer. Photoemission Studies of the Noble Metals. I. Copper. *Phys. Rev.*, 185:882, 1969.
- [22] D. H. Dowell, F. K. King, R. E. Kirby, and J. F. Schmerge. In situ cleaning of metal cathodes using a hydrogen ion beam. *Phys. Rev. ST : Accel & Beams*, 9:063502, 2006.
- [23] W.E. Spicer and A. Herrera-Gomez. Modern theory and applications of photocathodes. *Proc.SPIE Int.Soc.Opt.Eng.*, 2022:18–33, 1993.
- [24] P. Hofmann. Lecture Notes on Surface Science. <http://philiphofmann.net/surflec3/surflec011.html>.
- [25] Computational Electronic Structure Database (CompES). [http://caldb.nims.go.jp/index\\_en.html](http://caldb.nims.go.jp/index_en.html).
- [26] F. Le Pimpec et al. Results of the PSI Diode-RF Gun Test Stand Operation. In *IPAC2010, Kyoto, Japan*, 2010.
- [27] J.E. Sipe and J. Becher. Surface-plasmon-assisted photoemission. *J. Opt. Soc. Am*, 71(10):1286, 1981.
- [28] T. Tsang, T. Srinivasan-Rao, and J. Fischer. Surface-plasmon-enhanced multiphoton photoelectric emission from thin silver films. *Opt. Lett.*, 15:866, 1990.
- [29] O. Tüske. Photoémission Laser assistée par Plasmon de Surface. Technical report, CEA Saclay, 1997.
- [30] C. Guo. Surface-plasmon-enhanced photoelectron emission, 2010. [spie.org/documents/Newsroom/Imported/002935/002935\\_10.pdf](http://spie.org/documents/Newsroom/Imported/002935/002935_10.pdf).
- [31] H.J. Qian, J.B. Murphy, Y. Shen, C.X. Tang and X.J. Wang. Surface photoemission in a high-brightness electron beam radio frequency gun. *Appl. Phys. Lett.*, 97:253504, 2010.
- [32] D.Y. Li, L. Wang, W. Li. Effects of grain size from micro scale to nanoscales on the yield strain of brass under compressive and tensile stresses using a Kelvin probing technique. *Materials Science and Engineering, A* (384):355, 2004.
- [33] P. A. Anderson and A. L. Hunt. Effect of Oxygen on the Work Function of Barium. *Phys. Rev.*, 115(9):550–552, 1959.
- [34] M.E. Grubbs, M. Deal, Y. Nishi, and B.M. Clemens. The Effect of Oxygen on the Work Function of Tungsten Gate Electrodes in MOS Devices. *IEEE Electron Device Letters*, 30(9), 2009.
- [35] A. Lorusso, F. Gontad, A. Perrone, and N. Stankova. Highlights on photocathodes based on thin films prepared by pulsed laser deposition. *Phys. Rev. Special Topics - Accelerators and Beams*, AB 14:090401, 2011.
- [36] K. Nemeth, K.C. Harkay, M. van Veenendaal, L. Spentzouris, M. White, K. Attenkofer and G. Srajer. High-Brightness Photocathodes through Ultrathin Surface Layers on Metals. *Phys. Rev. Lett.*, 104:046801, 2008.

- [37] D.H. Dowell, I. Bazarov, B. Dunham, K. Harkay, C. Hernandez-Garcia, R. Legg, H. Padmore, T. Rao, J. Smedley and W. Wan. Cathode R&D for future light sources. *Nuclear Instruments and Methods in Physics Research A*, 622:685, 2010.
- [38] V.G. Tkachenko A.I. Kondrashev I.N. Maksimchuk. Advanced metal alloy systems for massive high-current photocathodes. *Appl. Phys. B*, 98:839–849, 2010.
- [39] T. Srinivasan-Rao, J. Fischer and T. Tsang. Photoemission studies on metals using picosecond ultraviolet laser pulses. *Journal of Applied Physics*, 69:3291, 1990.
- [40] C.P. Hauri, R. Ganter, F. Le Pimpec, A. Trisorio, C. Ruchert, and H.H. Braun. Thermal Emittance Reduction of Electron Beam from Metal Photocathodes. *Phys. Rev. Lett.*, 104 (234802), 2010.
- [41] A. Septier, F. Sabary, J-C. Dubek, A. Boumiz. Une Photocathode à réserve alcaline (Al-Li)-Ag-O-Li. *C.R. Acad. Sci. Paris*, 314 (serie II):569, 1992.
- [42] F. Le Pimpec, F. King, and R.E. Kirby. Electron conditioning of technical aluminium surfaces: Effect on the secondary electron yield. *Journal of Vacuum Science and Technology, A* (23):1610, 2005.
- [43] R. Ganter, PSI, private communication.
-

## List of Tables

1	Work function and associated wavelength for some bulk elements [16,17,18,19,20]	6
2	Parameters used to fit the QE data for Cu and Mg of Fig.6 [16,22]	9
3	Temperature increase of different metals when submitted to 10 $\mu\text{J}$ /pulse laser irradiation.	11

## List of Figures

- 1 Experimental vacuum chamber with a Cu cathode visible at its center surrounded by a Faraday cup (FC). A cold cathode compact vacuum gauge monitors the total pressure in the chamber. A conflat MgF<sub>2</sub> vacuum window closes the vacuum chamber. 3
- 2 Experimental setup, Electric diagram. The system encompasses an insert (photocathode) a Faraday cup (FC) surrounding it, a +/- 12 V battery powered power supply, and a K6514 Ammeter 3
- 3 The left figure (top) is the recorded voltage by the oscilloscope when the Mg cathode is illuminated by the Duetto<sup>®</sup> laser (355 nm, 200 kHz, 140 mW, ~10 ps), FC = +9 V. A mV corresponding to a nA of photo-emitted current. The right figure (top) is the recorded voltage by the oscilloscope when irradiating the same polished Mg cathode using the Topas<sup>®</sup> laser (260 nm, 1 kHz, 5 μJ, ~100 fs), FC is off. In both figures, the bottom plots are the traces of the recorded laser impulsion. 4
- 4 QE vs wavelength of two different polished (mirror-like) Cu samples. The FC is OFF. The QE are compared at a specific wavelength with QE data measured in two different accelerators. 6
- 5 QE vs wavelength of polished (non mirror-like) Mg#2. The FC is OFF. 7
- 6 QE vs wavelength of a polished (mirror-like) Cu#R4 sample (left plot) and of a freshly re-polished Mg#2 (right plot), using two laser pulse lengths 1 ps and 100 fs. The straight line are the fittings using equation 2 7
- 7 QE of Cu#R4 vs the FC voltage at set wavelength for a set Topas<sup>®</sup> energy in microJ. 8
- 8 Damages caused by laser exposition on polished but rough Mg# 2 11
- 9 Damages caused by laser cleaning on polished Mg in the combined Diode-RF gun (OBLA) 11

10	Electron Current extracted versus the Topas <sup>®</sup> laser energy at 253 nm for CuR2 and at 331 nm for CuR1. In both cases the FC is OFF.	12
11	Current (left) and QE (right) measured as a function of the Duetto <sup>®</sup> laser energy for two Cu samples and one Mg insert. Double-Photon absorption emission is responsible for electron emission For Cu the FC is on at +4 V and is off for the Mg insert.	14
12	QE and Current versus the FC bias of two polished mirror-like Cu samples	15
13	QE versus the FC bias of two polished Mg sample Mg# 2 (rough) and Mg # 7 (mirror-like)	15
14	QE evolution under Duetto irradiation for two polished Mg sample Mg#2 (rough) and Mg#7 (mirror-like). FC is off in all cases.	16
15	QE and Current evolution of Alli alloy during Duetto <sup>®</sup> exposition, in function of the FC bias voltage.	18
16	Alli current extracted in function of the Duetto <sup>®</sup> laser energy. FC is set at +4V.	19
17	QE and Current evolution of Al during Duetto <sup>®</sup> exposition, in function of the FC bias voltage.	19
18	Charge map (pC) evolution of the Cu photocathode (Left plot: initial charge map) after three months of Injector operation (right plot).	20
19	New Cu photocathode (Cu.3) QE evolution after three months of Injector operation. Comparison with the QE of the first cathode installed Cu.1 [43].	21
20	QE (left) and Current (right) measured from a Cu cathode (CuR2) using the Topas <sup>®</sup> laser with a 1 kHz repetition rate and with $\lambda=261$ nm	21